Wooten, Jr., *The 3-j and 6-j Symbols* (MIT Technology Press, Cambridge, Mass., 1959).
[25]M. J. Weber and R. W. Bierig, Phys. Rev. 134A, 1492 (1964), Table IV.
[26]J. B. Gruber and J. G. Conway, J. Chem. Phys. 32, 1531 (1960).
[27]G. H. Dieke, *Spectra and Energy Levels of Rare Earth Ions In Crystals* (Interscience, New York, 1968).
[28]B. R. Judd, Phys. Rev. 125, 613 (1962).
[29]S. A. Johnson, H. G. Freies, A. F. Schawlow, and W. M. Yen, J. Opt. Soc. Am. 57, 734 (1967).

PHYSICAL REVIEW B VOLUME 2, NUMBER 7 1 OCTOBER 1970

Nuclear Magnetic Resonance in the Cesium-Graphite Intercalation Compounds*

G. P. Carver†
Laboratory of Atomic and Solid State Physics, Cornell University, Ithaca, New York 14850
(Received 20 April 1970)

The C^{13} and Cs^{133} nuclear magnetic resonances have been studied in powdered samples of the cesium-graphite intercalation compounds at temperatures between 1.3 and 4.2 °K. The spin-lattice relaxation times and the line shapes of both nuclear species in the compounds and of the C^{13} nucleus in pure graphite were measured in an effort to determine the nature of the conduction-electron states in these substances. At 4.2 °K, using pulse techniques, the measured values of T_1 for C^{13} are 1.6 ± 0.3, 2.6 ± 0.4, 3.9 ± 0.5, 5.6 ± 0.5, 7.6 ± 0.8, and 30 ± 5 min in C_8Cs, $C_{24}Cs$, $C_{36}Cs$, $C_{48}Cs$, $C_{60}Cs$, and pure graphite, respectively. Both the Salzano-Aronson binding model for the compounds and a tight-binding extension to the Slonczewski-Weiss band model for graphite are shown to account qualitatively for the cesium concentration dependence of the C^{13} T_1's. None of the usual relaxation mechanisms is conclusively identified with the relatively short C^{13} T_1's. The temperature dependence also remains unaccounted for. Echo techniques at helium temperatures establish the shape of the 500-G-wide cesium quadrupolar spectrum in C_8Cs at 1.3 °K. The measured quadrupolar splitting is 16.8 ± 1 kHz. The Knight shift for cesium in C_8Cs is measured to be $(0.29 \pm 0.01\%)$, independent of temperature from 300 to 1.3 °K. In $C_{24}Cs$ and $C_{36}Cs$, the Knight shift was zero within $\pm 0.02\%$. The experimentally measured T_1 for Cs^{133} in C_8Cs was 7.5 ± 0.5 sec, while the T_1's in $C_{24}Cs$ and $C_{36}Cs$ were 27 ± 6 and 48 ± 10 min, respectively. The Cs^{133} Knight-shift and relaxation-time results support the view that the cesium is partially ionized in C_8Cs and completely ionized in the cesium-poorer stages.

I. INTRODUCTION

The techniques of nuclear magnetic resonance (NMR) have provided detailed information about interactions between nuclei and their environments in a variety of physical systems. This paper reports on the use of these techniques to study one member of an unusual group of crystalline, metal-like compounds, the alkali-graphite intercalation compounds.

The crystal structure of these compounds is well known.[1-3] Their static susceptibilities have been measured and are paramagnetic, in contrast to the large diamagnetism of pure graphite.[4] Electrical conductivity in the potassium-graphite system increases with increasing alkali concentration, although with different rates in the two different crystal directions.[5] Thermodynamic properties, such as energies of formation and alkali vapor pressures, have been measured.[6] The most alkali-rich stages of the cesium, rubidium, and potassium compounds have been observed to undergo a superconducting transition.[7] The critical field is anisotropic. More recently, an expansion of the carbon-carbon bond length with increasing alkali content has been observed in the potassium-graphite system.[8]

In general, experimental results are consistent with the assumption that there is a transfer of electronic charge from alkali to the graphite layers. However, little detailed information about the nature of the resulting electronic states is available. The electrostatic binding model of Salzano and Aronson[9,10] successfully accounts for the bonding energies of all but the two most alkali-rich stages. However this model is not sensitive to the nature of the electronic states.

We report here on the low-temperature magnetic resonance properties of graphite and the cesium-graphite system. The only previous observation of magnetic resonance in these compounds is the work of Jensen, O'Reilly, and Tsang.[11] They observed the cw peak of the Cs^{133} line in C_8Cs and $C_{24}Cs$ – a "line" that in this study is shown to be the central peak of a quadrupolar broadened powder pattern. Their quoted values for the cesium Knight shift are in disagreement with results presented here.

Section II is devoted to a brief discussion of the

properties of graphite and the alkali-graphite intercalation compounds. Section III describes the materials, the methods of sample preparation, and the experimental equipment. The experimental program, the data, and the results are presented in Sec. IV. Section V is the analysis and discussion of the results.

II. MATERIALS

A. Graphite

The carbon atoms in graphite are arranged in planes, each plane a two-dimensional network of hexagons with edge 1.42 Å. The planes are separated by 3.37 Å. Intraplanar bonding may be described by sp^2 bonding orbitals with the remaining p_z electron of each carbon atom in a π orbital delocalized around the network of "benzene rings." Interplanar bonding is of the van der Waals type.

Since the planes are relatively distant and weakly interacting, early band-structure calculations[12] used two-dimensional tight-binding approximations. However, the three-dimensional Slonczewski-Weiss model[13] has been used more successfully to explain the results of a large variety of experiments.[14]

More complete discussions are provided in the review by Haering and Mrozowski,[15] and in the monograph by Ubbelohde and Lewis.[2]

B. Alkali-Graphite Compounds

The alkali-graphite "intercalation" or "lamellar" compounds are crystalline materials with the metal atoms in layers between graphite planes.[1-3] At least six well-defined "stages" have been identified in the cesium-graphite system. (Rubidium and potassium form similar stages.) The cesium-graphite compounds have ideal formulas C_8Cs, $C_{24}Cs$, $C_{36}Cs$, $C_{48}Cs$, and $C_{60}Cs$. (A stage with the formula $C_{10}Cs$ has been reported, but it is unstable below 324 °C.[6]) C_8Cs has a metallic brownish-gold color, $C_{24}Cs$ is a deep blue, and the more cesium-poor stages range from blue-black to almost black. They decompose rapidly in air.

The crystal structure of the intercalation compounds was established by Rudorff and Schulze.[4] Recently, more accurate x-ray studies[8,16] have slightly modified the original model.

The sequences of metal and carbon layers for the compounds are shown in Fig. 1. C_8Cs has a layer of cesium atoms between every pair of graphite layers. $C_{24}Cs$ has a cesium layer after every second graphite layer. This pattern is extended, so that in $C_{60}Cs$ a cesium layer comes after every fifth graphite plane. The pure graphite interlayer spacing expands to accommodate the cesium layer.

The concentration of cesium per alkali layer is highest in C_8Cs, but remains constant, at two-thirds of the C_8Cs value, in each of the other stages. Each

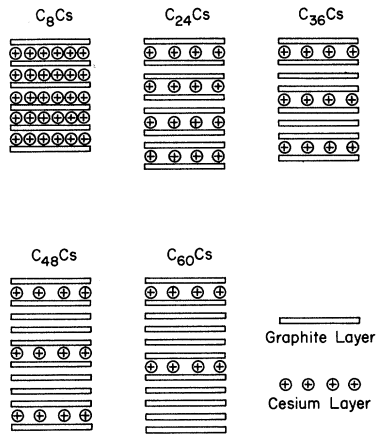

FIG. 1. Metal-layer–graphite-layer stacking sequences for the cesium-graphite intercalation compounds.

cesium nucleus is surrounded by 12 nearest-neighbor carbon atoms.

The Salzano-Aronson binding model successfully accounts for the bonding energies and other thermodynamic properties of the compounds.[9,10] In this model the alkali valence electron is ionized into a conduction band associated with those graphite planes immediately adjacent to an alkali layer. The bonding mechanism is the electrostatic attraction between the positive alkali atoms and the adjacent negatively charged sheets of graphite. The Salzano-Aronson model is unable to describe phenomena directly related to the nature of the electronic states.

Measurements of the thermoelectric power have been used to support a model for the bands in the potassium compounds by assuming that these are merely doped graphite systems.[17]

In general, experimental data support the notion that formation of the compounds involves an electron transfer mechanism from the alkali to the host graphite lattice.[5,18] However, no detailed description of the band structure nor of the electronic wave functions has been published.

III. EXPERIMENTAL DETAILS

A. Materials

The graphite used to make the samples was National spectroscopic graphite powder, grade SP-2, supplied by the Union Carbide Corp. Total impurity content is guaranteed less than 6 ppm. Particle size is less than 35 μ. SP-2 powder has been heat treated in excess of 3000 °C and is described as "well graphitized."

The alkali metals were obtained from MSA Research Corp. in 2-g ampoules. Purity is $3N^+$. The

metal was used directly from the ampoules.

B. Sample Preparation

Samples were prepared by heating weighed amounts of metal and outgassed graphite powder in sealed Pyrex tubes. The atmosphere inside the tubes was helium gas at about $\frac{1}{2}$-atm pressure. The tubes were gently heated so that the reaction, aided by vigorous shaking, was complete in just a few minutes. The final products were C_8Cs and unreacted graphite (except in the case of the preparation of C_8Cs itself, when there was no excess graphite).

The reaction tubes were kept in a tubular furnace for several days at about 300 °C. The final contents were a uniform color appropriate to the desired compound. No precise analysis was performed. The several day heating period was longer than that reported necessary for complete annealing.[6]

The sample material was mixed in outgassed Dow Corning 704 fluid (for particle separation) and injected into the sample tubes.

All operations with exposed materials were performed in a glove box under a dry helium atmosphere.

C. Experimental Apparatus

Low-temperature measurements were performed on a crystal controlled-pulsed spectrometer. The gated oscillator and transmitter circuitry were homemade.[19] The pulsing sequences were generated by Tektronix type-162 waveform generators and type-163 pulse generators. The receiver consisted of an Arenberg Model PA-620 tuned preamplifier and Model WA-600B wide band amplifier. The samples, in Pyrex tubes, were mounted in a conventional tuned crossed-coil configuration. Achievable H_1's were about 50 G in the rotating frame, as measured by the 90° pulse length required for a proton resonance.

The samples were immersed in the liquid-helium bath. Temperature was monitored both by resistive techniques and by oil and mercury manometers connected to the helium Dewar.

Room-temperature measurements were taken on a cw spectrometer consisting of a crystal oscillator stabilized Varian model V 4210 A rf unit, Varian model V 4230 B NMR probes, an audio oscillator, an audio amplifier, an Ithaco model 353 lock-in amplifier, and a Moseley model 135 M x-y recorder.

The magnetic field was supplied by a Harvey Wells magnet with 12-in. -diam pole faces and a 3-in. gap. The field inhomogeneity, less than 5 parts in 10^6 at 2 kG, was minimized by maximizing the Bloch decay time for a doped water sample.

The field was measured with a Harvey Wells gaussmeter model G-501 and a Beckman-Berkeley model 7175 N frequency counter.

A boxcar integrator was used to obtain the cesium quadrupolar line shape in C_8Cs.

The rf frequency was 8.5 MHz in a field of 8 kG for the C^{13} resonance and 5.5 MHz in 10 kG for the Cs^{133} resonance.

IV. RESULTS

A. T_1 for C^{13} at Low Temperature

Experimentally measured values of the spin-lattice relaxation time T_1 for the C^{13} nucleus in the compounds and in pure graphite are shown in Fig. 2(a). The data were obtained with the pulse spectrometer using conventional 90°-τ-90° pulse sequences. The signal height was measured at standard intervals along the free induction decay (FID) after the second pulse. The sum of these heights was taken as a measure of the recovered magnetization M at time τ. T_1 was obtained from the slope of a plot of $\ln(M_0 - M)$ against τ, where M_0 is the equilibrium magnetization. M_0 was measured with the condition $\tau \gg T_1$.

The uncertainty in measurements of the signal amplitude was estimated by visual inspection of the signal-to-noise ratio. The uncertainties in the slope of the T_1 graphs were obtained by graphical methods. The error estimate is probably rather generous.

Data on the C^{13} T_1 in C_8K are given in Fig. 2(b).

B. T_1 for C^{13} at Room Temperature

The room-temperature value of T_1 for C^{13} in pure graphite was established by a standard fast-passage experiment with the cw spectrometer. The measured value of T_1 is 89 ± 10 sec and is shown along with the graphite low-temperature T_1 data in Fig. 3. If T_1 was fit to a straight line over the entire temperature range the slope would be -0.7, falling between the metallic behavior, $T_1 \propto T^{-1}$, and the semiconducting behavior, $T_1 \propto T^{-1/2}$.

The error estimate for the fast-passage value for T_1 comes from an analysis similar to that used for the low-temperature pulse data.

C. C^{13} Line Shapes

Table I gives the measured values for T_2^* and T_2 for the C^{13} resonance in the cesium compounds and in pure graphite. T_2^*, the $1/e$ falloff time in the FID, was obtained by graphing the signal heights at intervals along the FID against time on a semilog plot.

T_2, the inverse dipolar linewidth, was measured by the spin-echo amplitudes after the usual 90°-variable τ-180° pulse sequence.

The C^{13} line shape in pure graphite was Lorentzian (exponential FID) while the line shapes in the

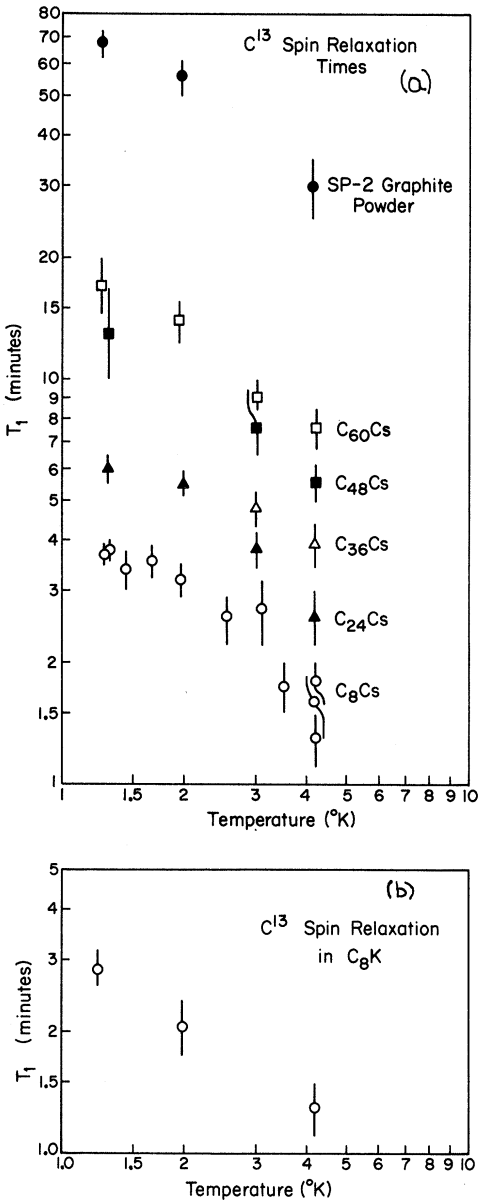

FIG. 2. C^{13} spin-lattice relaxation time as a function of temperature for (a) graphite and the cesium-graphite intercalation compounds and (b) C_8K.

compounds were almost Gaussian ("almost Gaussian" FID). All dipolar T_2 plots from spin-echo data appeared to be pure exponentials.

The C^{13} signal was observed in one sample of C_8K and the linewidth data are included in Table I.

D. Cs^{133} Quadrupolar Line Shape and Echo Spectrum in C_8Cs

The Cs^{133} resonance in C_8Cs is split by quadrupolar interactions. In a powder sample the orientation-dependent satellite lines are broadened and are not easily observed. The cw spectrum at room temperature is shown in Fig. 4. The decrease in intensity from that for the Cs^{133} resonance in cesium metal is about a factor of 5 and the Cs "line" is thus identified with the central peak of a spin-$\frac{7}{2}$ quadrupole spectrum.[20] (This statement also applies to Jensen, O'Reilly, and Tsang's[11] observation of the cw line at 4.2 °K.)

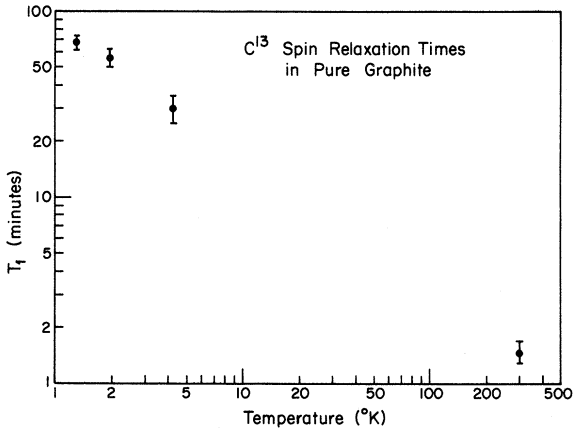

FIG. 3. T_1 for C^{13} in pure graphite. The room-temperature point was obtained by a fast passage experiment.

At low temperature, on the pulse spectrometer, the entire quadrupole spectrum was graphed by the method used by Narath for lanthanum metal.[21] The output from a boxcar integrator, gated at the peak of the echo at 2τ, was graphed by an x-y recorder while the magnetic field H_0 was swept through the resonance line. The pulse sequence was $90°$-τ-$\approx 45°$. (Pulse lengths are defined by the metallic $90°$ pulse length.) τ was as short as possible, limited by the 20-μsec receiver deadtime. The second pulse length was chosen for maximum echo height.

The spectrum at 1.3 °K is shown in Fig. 5. The frequency shift between peaks has the value 8.4

TABLE I. C^{13} Linewidths at 1.3 °K.

Material	T_2^{*a} (msec)	ΔH^* (G) (Inferred width at half-max.)	T_2 (msec)	ΔH (G) (Inferred width at half-max.)
Pure graphite	0.33	0.92	4.1	0.072
C_8Cs	0.43	1.0	1.6	0.19
$C_{24}Cs$	0.59	0.73		
$C_{60}Cs$	0.56	0.77		
C_8K	1.2	0.36		

[a] T_2^* for C^{13} in the compounds was almost Gaussian. T_2^* in pure graphite and all T_2's were exponential. The appropriate expressions for ΔH were used depending on whether the decay was Lorentzian or Gaussian.

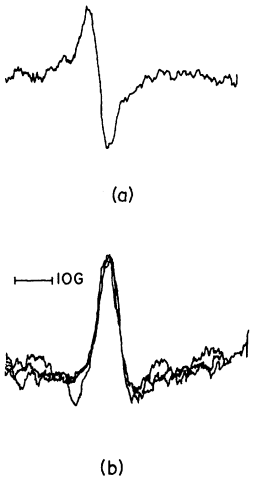

FIG. 4. cw spectrum of Cs^{133} in C_8Cs in the (a) absorption mode and (b) dispersion mode at room temperature. The modulation field was 8-G p-p. The resonant frequency was 5.5 MHz.

± 0.6 kHz.

The Cs^{133} FID, arising from the central line, may be associated with a resonance line shape intermediate between Lorentzian and Gaussian with a linewidth of about 8 G. This inferred width is in accord with the width of the central peak observed by cw methods.[11] A typical signal at equilibrium magnetization is shown in Fig. 6(a).

Quadrupolar echoes were observed at 2τ and 3τ. (Poor signal-to-noise ratio prevented detection of all seven quadrupolar echoes.) The 2τ echo contains contributions from all satellites with the outer satellites contributing the narrower components.[22] The 3τ echo is due to the inner satellites, the $\frac{3}{2} \leftrightarrow \frac{1}{2}$ and $-\frac{3}{2} \leftrightarrow -\frac{1}{2}$ transitions. An estimate of the 3τ echo duration gives a half-width of 30 ± 6 G for the inner satellites.

E. T_1 for Cs^{133} in C_8Cs at Low Temperature

The available rotating field H_1 is small compared to the total quadrupole linewidth. Under these circumstances, a single pulse would "heat" only a small part of the total line. However, saturation of the entire line may be brought about by a series, or "comb," of closely spaced pulses. If the field is positioned on the central peak, saturation comes about through electron-coupled transitions between the central peak and the satellites.

In the present work, sample heating (appearing as a reduction in the amplitude of the FID after a given time interval) was observed before complete saturation could be achieved. Yet a value for T_1 was obtained by observing the recovery of the magnetization, as measured by the FID due to the central peak, even though the spin system was not saturated. Under these conditions, the recovery of the magnetization contains initially faster components caused by transitions from the satellites to the central peak. After some time, all components of the line reach an equal spin temperature and the entire spin system recovers toward equilibrium magnetization at a relaxation rate which may be taken as the average. This average, or intrinsic, T_1 may be extracted from the asymptotic value of the recovery of the magnetization.

A plot of $\ln[(M_0 - M)/M_0]$ against time after a nonsaturating train of pulses is shown in Fig. 7. The ratio of the initial relaxation time of 0.3 ± 0.1 sec to the long-time relaxation time of 7.5 ± 0.5 sec agrees with the ratio of 28 between the fastest and asymptotic relaxation rates for a spin-$\frac{7}{2}$ quadrupole line, as calculated by Narath.[21]

F. Line Shapes and T_1's for Cs^{133} in $C_{24}Cs$ and $C_{36}Cs$

Under similar conditions as described above for the case of C_8Cs, the cesium line in $C_{24}Cs$ and $C_{36}Cs$ behaved as though it were saturated after only a single 90° pulse. (Poor signal-to-noise ra-

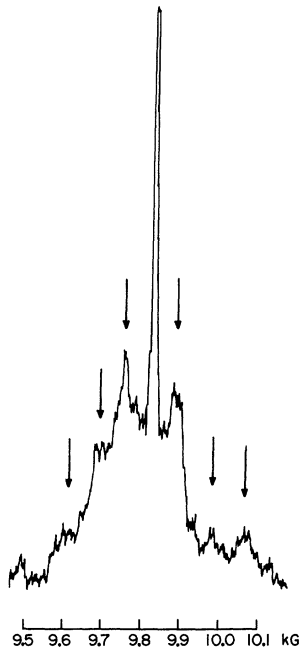

FIG. 5. Cs^{133} quadrupole line in C_8Cs at 1.3 °K. The spectrum is a record of the amplitude of the echo at 2τ as a function of the magnetic field. H_1 was reduced to ≈ 20 G for greater resolution.

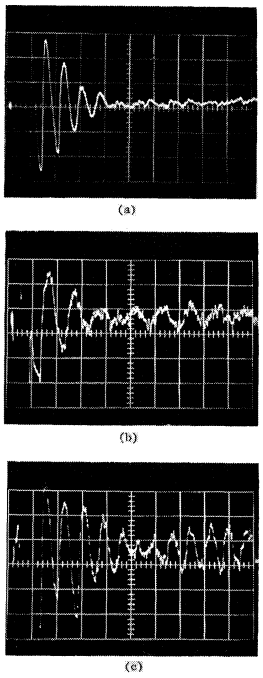

FIG. 6. Cs^{133} FID, slightly off resonance, at full magnetization in (a) C_8Cs, (b) $C_{24}Cs$, and (c) $C_{36}Cs$ at 1.3 °K. The time scale is 50 μsec per large division.

tio precluded observation of the Cs^{133} signal in the higher stages.) The measured T_1's were 27 ± 6 and 48 ± 10 min in $C_{24}Cs$ and $C_{36}Cs$, respectively. No echoes could be observed and, as shown in Fig. 8, there is little evidence for more than a single relaxation rate. A 90°-τ-90° pulse sequence was used.

The FID's for these compounds are shown in Figs. 6 (b) and 6 (c).

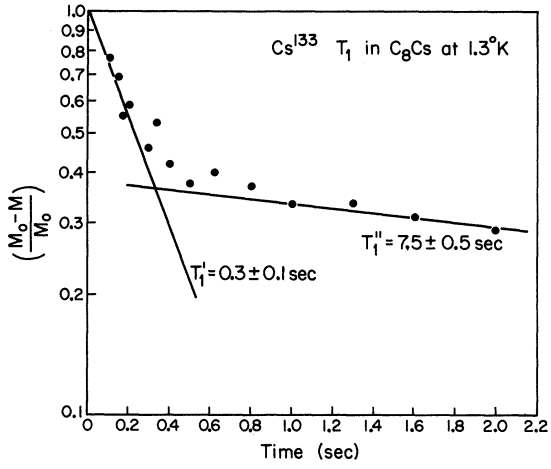

FIG. 7. Recovery of the Cs^{133} magnetization in C_8Cs at 1.3 °K after a nonsaturating comb of ten pulses, 5.5 μsec each.

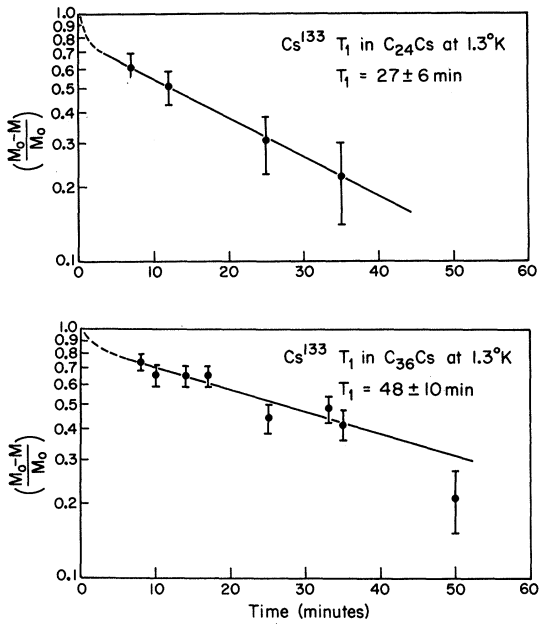

FIG. 8. Recovery of the Cs^{133} magnetization in (a) $C_{24}Cs$ and (b) $C_{36}Cs$ at 1.3 °K after a single 90° pulse of 5.5-μsec duration.

G. Cs^{133} Knight Shift

The field positions of the Cs^{133} resonances in C_8Cs and $C_{24}Cs$ were measured relative to the Cs^{133} signal in a pure-metal sample on the cw spectrometer at room temperature. The lines were recorded on the same trace by switching samples. One such sweep through the C_8Cs and $C_{24}Cs$ dispersion lines is shown in Fig. 9. The results, averaged over many such measurements, are presented in Table II. The data are in disagreement with that of Jensen, O'Reilly, and Tsang[11] who measured equal shifts of 0.25% in both C_8Cs and $C_{24}Cs$, and in $C_{48}Cs$. They also observed a line, not detected in this study, which was shifted by 0.4% in samples of C_8Cs.

The relative Knight shifts do not show any measurable temperature dependence. The central peaks of the resonances were observed to have the same relative field values, within an uncertainty of about 2 G, at low temperature on the pulse spectrometer.

V. DISCUSSION OF RESULTS

A. C^{13} Nuclear Relaxation

No simple, yet comprehensive, model has been found which satisfactorily accounts for all aspects of the spin-lattice relaxation data. However, even though the nature of the basic C^{13} relaxation mechanism remains unknown, certain features of the T_1

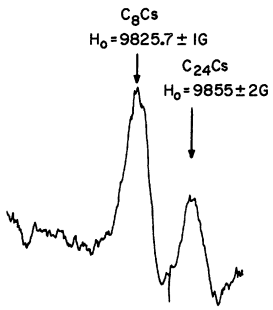

FIG. 9. Room-temperature Cs^{133} dispersion lines at 5.5 MHz in C_8Cs and $C_{24}Cs$ recorded on a single sweep. The indicated field positions are the results of several measurements of the difference in field positions between the Cs^{133} line positions in cesium metal, C_8Cs, and $C_{24}Cs$. The Cs metal line was used as the reference. The $C_{24}Cs$ line falls at the expected unshifted Cs^{133} resonance, based on the known Knight shift of the metal line.

data are in limited accord with certain models and some discussion of this accord will be given later in this section.

1. *Possible* C^{13} *Relaxation Mechanisms*

All relaxation processes known to us and consistent with a system of spin-$\frac{1}{2}$ nuclei are found to be too weak to account for the data. Some of the difficulties encountered in explaining the data are discussed in the following list of possible relaxation mechanisms.

Direct dipole-dipole relaxation to the Cs^{133} *nuclei.* It is well known that the spectral density of fluctuations in local magnetic fields arising from lattice vibrations is very small at the (relatively) low nuclear Larmor frequencies. Moreover, if local field fluctuations at C^{13} sites were to come from the reorientation of Cs^{133} nuclei in the course of nuclear relaxation, the effect is negligibly weak. This relaxation rate may be estimated from an expression for T_1 in liquids due to local field fluctuations caused by the thermal motion of nuclear moments.

Impurity relaxation. Impurity relaxation is unlikely since the various C^{13} T_1's in the compounds display the same unusual temperature dependence as does T_1 in pure graphite.

Relaxation by s-state electrons. The relaxation of nuclei in a metal by coupling to the s-state conduction electrons is given by the familiar expression

$$\frac{1}{T_1} = \frac{64}{9}\pi^3\hbar^3\gamma_e^2\gamma_n^2\langle |u_k(0)|^2\rangle_{E_F} \mathfrak{D}^2(E_F)kT. \quad (1)$$

The experimental value of T_1T for C^{13} in C_8Cs, when used with Eq. (1), predicts a value of $\langle |u_k(0)|^2\rangle_{E_F}$ which is greater than the value of that quantity for Li^7 in lithium metal. Such a situation is quite improbable, and argues against the identification of s-state electrons as the source of relaxation, in agreement with the Slonczewski-Weiss Model.[13]

Nuclear dipole-electron dipole relaxation. In the Slonczewski-Weiss band model for graphite, the only free-carrier states are linear combinations of p_z orbitals. An expression for T_1 using p_z wave functions and the dipolar Hamiltonian was calculated[23] following the method of Slichter for the Fermi contact interaction.[24] The result, similar to that of Narath and Wallace,[25] is

$$\frac{1}{T_1} = \frac{4\pi}{25}\gamma_e^2\gamma_n^2\hbar^3\left\langle\frac{1}{r^3}\right\rangle^2 \mathfrak{D}^2(E_F)kT. \quad (2)$$

For graphite, $\mathfrak{D}(E)$ is taken as[26] 0.006 (atom eV)$^{-1}$ and $\langle 1/r^3\rangle$ as 1.692 in a.u.[27] The resulting value for T_1 is 32.4 days at 4.2 °K for pure graphite. The measured value is 30 min. This electronic process is also too weak for the compounds if calculated values for the density of states in the compounds (Eq. 11) are used.

Orbital relaxation by p-state electrons. Even in the most favorable case, with all three p-states equally populated, orbital relaxation is only a factor of 3 more effective than dipolar relaxation.[28]

Relaxation by core polarization. Generally, relaxation by core polarization is less effective than relaxation by ordinary contact interaction.

2. *Cesium Concentration Dependence of* C^{13} *Relaxation*

Models based on the Salzano-Aronson binding model[9] and on the Slonczewski-Weiss band model for graphite[13] are each able to correctly predict the C^{13} T_1 dependence on cesium concentration. Both models include the assumption that the relevant effect on T_1 of the intercalation of cesium is a change in the electronic density in the compounds. However, the models represent completely opposite points of view so far as the electron spatial distribution is concerned.

Salzano-Aronson binding model. In the Salzano-Aronson model the electrons are treated as being

TABLE II. Cesium Knight shifts in C_8Cs and $C_{24}Cs$.

	Proton freq. in MHz at center of room temp. dispersion line at 5.5 MHz	Measured shift in G from Cs metal line	$\Delta H/H$ based on known metallic Knight shift
Cs metal	41.3281 ± 0.0002	...	(1.49%)
C_8Cs	41.829 ± 0.003	117.7 ± 0.9	(0.29 ± 0.01%)
$C_{24}Cs$	41.930 ± 0.009	147 ± 2	(0 ± 0.02%)

localized on the two "filled" graphite layers adjacent to each metal layer. (With the simplest picture, $C_{60}Cs$, for example, has two graphite layers with the same electronic density as those of $C_{24}Cs$ for every three layers of "pure" graphite.)

In this model all effective relaxation of C^{13} nuclei in the compounds would take place on the "filled" layers since the pure graphite T_1 is so much longer. Unfilled layers would be relaxed via spin-spin interactions characterized by some diffusion time. This diffusion time will be on the order of T_2. Hence the spin system will be in thermal equilibrium during the relaxation and the bottleneck is the C^{13} relaxation in the filled layers.

This conclusion leads directly to a prediction for the expected T_1 dependence on cesium concentration for the compounds $C_{24}Cs$ through $C_{60}Cs$, because the filled layers have identical electronic character in this model. (C_8Cs has a higher concentration of metal per alkali layer, so it is not included in this simple analysis.)

Since there was no evident difference in equilibrium magnetization among the various samples, the conclusion is that all nuclei were being detected. The observed total magnetization M may be thought of as resulting from the combined contributions of the filled layers and the unfilled or "reservoir" layers

$$M = M_F + M_R \quad . \tag{3}$$

Since the relaxation takes place only on the filled layers, both M_F and M_R would relax with the same net relaxation time,

$$M_F = M_{F0}\,(1 - e^{-t/T_1}) \quad , \tag{4a}$$

$$M_R = M_{R0}\,(1 - e^{-t/T_1}) \quad . \tag{4b}$$

The subscript "0" refers to equilibrium magnetization. At any time t one has

$$M_R = (M_{R0}/M_{F0})\,M_F \quad . \tag{5}$$

The relaxation of the total magnetization is given by

$$\frac{dM}{dt} = \frac{M_{F0} - M_F}{\tau} \quad , \tag{6}$$

where τ is the intrinsic relaxation rate associated with the filled layers (or alternately with $C_{24}Cs$). Substituting for M, one has

$$\left(1 + \frac{M_{R0}}{M_{F0}}\right)\frac{dM_F}{dt} = \frac{M_{F0} - M_F}{\tau} \quad . \tag{7}$$

The solution

$$M_F = M_{F0}[1 - \exp - t/\tau\,(1 + M_{R0}/M_{F0})] \tag{8}$$

identifies the sample T_1. That is

$$T_1 = \frac{M_{F0} + M_{R0}}{M_{F0}} \quad , \quad \tau = \frac{M_0}{M_{F0}}\,\tau \quad . \tag{9}$$

Thus, the C^{13} relaxation time for a given sample would be inversely proportional to the fraction of layers which are filled since the equilibrium magnetization is proportional to the numbers of nuclei. In other words, T_1 would be directly proportional to $\frac{1}{24}n$, where $n = 24$, 36, 48, or 60. Table III gives the predicted C^{13} T_1 ratios along with the measured T_1's for $C_{24}Cs$ through $C_{60}Cs$ at 4.2 °K.

Slonczewski-Weiss band model. Explicit dependence of T_1 on the band structure of a crystal arises through the density of states $\mathfrak{D}(E)$. Assuming the intercalation of cesium directly determines an electron density which is *uniform throughout the crystal*, the relationship between cesium concentration and T_1 may be obtained through an expression for $\mathfrak{D}(E)$. Implicit in this assumption of relaxation by spatially distributed free electrons is the fact that each C^{13} nucleus in the crystal has the same relaxation time.

The density of states in the compounds as a function of electron density is derived in the Appendix through a tight-binding approximation to the Slonczewski-Weiss model for the graphite band structure. The result is

$$\mathfrak{D}(E) = (2/\sqrt{3}\,\pi\,\gamma_0^2)\,[E - \tfrac{1}{2}(\Delta + \gamma_2)\,] \tag{10}$$

or

$$\mathfrak{D}(E) = 0.274N^{1/2} \quad , \tag{11}$$

where N is the number of donor electrons per carbon atom.

Since $1/T_1 \propto \mathfrak{D}^2\,(E)$ and $N = 1/n$, the electron-concentration dependence of this spatially nonlocalized electron model gives the same result as the localized electron analysis based on the Salzano-Aronson model.

The T_1's given by $\mathfrak{D}(E)$ from Eq. (11), for all the compounds including C_8Cs, are given in Table III.

TABLE III. Expected T_1 and χ ratios.[a] The underline entries are those appropriate only to the discussion of the Salzano-Aronson Model.

Compound	C^{13} T_1 at 4.2 °K (minutes)	χ (10^{-6} cgs units)	$\frac{T_1}{T_1 \text{ for } C_{24}Cs}$ (experiment)	$\left(\frac{\chi[C_{24}Cs]}{\chi}\right)^2$	Theory[a]
C_8Cs	1.6	1.0	0.62	0.87	0.56[b]
$\underline{C_{24}Cs}$	$\underline{2.6}$	8.7	$\underline{1.00}$	1.00	$\underline{1.00}$
$\underline{C_{36}Cs}$	$\underline{3.9}$	8.5	$\underline{1.5}$	1.1	$\underline{1.5}$
$\underline{C_{48}Cs}$	$\underline{5.6}$	5.7	$\underline{2.2}$	2.3	$\underline{2.0}$
$\underline{C_{60}Cs}$	$\underline{7.6}$	4.0	$\underline{2.9}$	4.7	$\underline{2.5}$

[a] The last three columns should be proportional to $\{[\mathfrak{D}(E) \text{ for } C_{24}Cs]/\mathfrak{D}(E)\}^2$.

[b] The theoretical value for C_8Cs is corrected for 55% ionization.

The static susceptibilities[4] C_nK are also given in Table III. The static susceptibility should be just the Pauli susceptibility and would therefore be proportional to $\mathfrak{D}(E)$, if one neglects diamagnetic corrections.

It should be noted, however, that numerical values for $\mathfrak{D}(E)$ for the compounds, calculated from Eq. (11), are larger than those inferred from the measured values of T_1 and the known density of states in pure graphite.[23]

"Localized" versus "nonlocalized" electrons. The agreement, on the cesium-concentration dependence of the values of T_1 in the compounds, between the above models is purely accidental. The susceptibility data of Rudorff and Schulze[4] show that χ is not merely an algebraic average between paramagnetic "filled" layers and diamagnetic graphite layers. These data and the carbon-carbon bond-length expansion data of Nixon and Parry[8] provide a clear choice in favor of a nonlocalized electron model. Thus, the treatment based on an extension to the Slonczewski-Weiss model would be the more suitable one.

3. *Temperature Dependence of* C^{13} T_1

It is not possible at this time to account for the observed temperature dependence in either the compounds or pure graphite. It is difficult to imagine how experimental artifacts such as rf heating or cesium-introduced paramagnetic impurities could produce the flattening of the curves at the lower temperatures, since these mechanisms would be greatly different or even absent in pure graphite. Yet it is clear from Fig. 2 that the same temperature dependence, to within experimental uncertainty, is obtained for T_1 in each sample.

In addition, there is no experimental evidence that sample temperatures varied from those of the bath. The equilibrium magnetization was found to be inversely proportional to (bath) temperature for a C_8Cs sample. Small effects of multiple-pulse rf heating could be observed, but only after tens of 90° pulses – a situation alien to the normal experimental program.

Finally, it should be observed that the data approximately follow a metallic $T_1 \propto T^{-1}$ dependence between 2 and 4.2 °K.

4. *Meditations*

It is fairly evident that none of the ordinary electron-nucleus or nucleus-nucleus interactions are adequate to explain the relaxation of the C^{13} spin system. Perhaps some more complicated or unique mechanism(s) is responsible. For example, the possibility that both C^{13} and Cs^{133} relaxations are due to coupling to the same, unidentified, fluctuating internal magnetic field may be considered.

Generally, a nuclear relaxation rate W may be expressed as

$$W = 1/T_1 = |\langle \alpha | \mathfrak{K}(t) | \beta \rangle|^2 J(\omega_{\alpha\beta}) \ , \qquad (12)$$

where $\mathfrak{K}(t)$ is the Hamiltonian describing a time-dependent coupling between initial and final spin states and $J(\omega_{\alpha\beta})$ is the usual spectral density function. If the coupling to the nuclear spins is due to a fluctuating magnetic field H_{loc} one has

$$1/T_1 \propto \gamma_n^2 H_{loc}^2 J(\omega_{\alpha\beta}) \ . \qquad (13)$$

Assuming a constant $J(\omega_{\alpha\beta})$, the ratio of $T_1(C^{13})$ to $T_1(Cs^{133})$ would be

$$T_1(C^{13})/T_1(Cs^{133}) = (\gamma_{Cs^{133}}/\gamma_{Cs^{133}})^2 = 0.27 \ . \qquad (14)$$

Experimentally, the ratio in $C_{24}Cs$ at 1.3 °K is

$$T_1(C^{13})/T_1(Cs^{133}) = 6 \text{ min}/27 \text{ min} = 0.22 \ , \qquad (15)$$

and in $C_{36}Cs$ at 1.3 °K is

$$T_1(C^{13})/T_1(Cs^{133}) = 9 \text{ min}/48 \text{ min} = 0.18 \ . \qquad (16)$$

(The T_1 for C^{13} in $C_{36}Cs$ was obtained by interpolation in Fig. 2.) The possibility of a common relaxation mechanism is certainly not excluded.

The ratio is quite different in C_8Cs, but it would appear from other data that C_8Cs is distinct from the other compounds in a number of other ways as well (see Sec. V D).

B. C^{13} Line Shapes

The carbon linewidths were given in Table I. Many of the experimental features may be understood on the basis of the carbon nuclear environments in the different compounds.

1. *Pure Graphite* T_2^*

The pure graphite linewidth at half-maximum was obtained from the FID on the assumption that the line shape is Lorentzian. For a polycrystalline powder sample, the line shape is determined by the anisotropic diamagnetism of graphite. The nature of the effect is similar to that arising from an anisotropic Knight shift. An approximate calculation, parallel to that for the anisotropic Knight shift, gives a lineshape in reasonable agreement with the measured value.[23]

2. *Pure Graphite* T_2

The pure graphite dipolar linewidth, which was determined from a spin-echo experiment, compares favorably with an estimate for the dipolar broadening in a magnetically dilute system. (In pure graphite, the 1.1% abundant C^{13} nuclei are the only nuclear dipoles.)

3. C^{13} *Line in* C_8Cs

The C^{13} line in C_8Cs, inferred from the FID, was

almost Gaussian. The broadening is due mostly to the static cesium dipolar field. Gaussian line shapes are expected in systems with the dipole concentration (now both C^{13} and Cs^{133} nuclei) greater than 0.1.

The echo T_2 in C_8Cs is shorter (implying a broader resonance line) than in the case of pure graphite. It is likely that the broadening of the C^{13} dipolar line in C_8Cs over the dipolar line in pure graphite is caused by mutual spin flips among the cesium nuclei. Cesium-cesium spin flips would create a varying field at the C^{13} nuclear sites which would limit the phase memory of the C^{13} nuclei, i.e., put an upper limit on the C^{13} T_2. An estimate of the period of this varying field, the cesium dipolar T_2, is not experimentally available because of quadrupolar effects. (The metallic Cs^{133} second moment[29] is consistent with a value of T_2 of about 1 msec.)

4. C^{13} *Line in* C_8K

The much narrower line, inferred from the FID, in C_8K (compared to C_8Cs) would be due to the smaller potassium dipolar moment.

C. Cesium Quadrupole Line

The Cs^{133} nucleus has spin $I=\frac{7}{2}$. The positions of the $2I$ lines, at maximum splitting, due to the quadrupolar interaction are given by the relation

$$H_{m\to m-1}=H_0+(\pi/\gamma_n)\,(m-\tfrac{1}{2})\,\nu_Q\ , \tag{17}$$

where $H_{m\to m-1}$ is the field position of the transition between the m and $m-1$ magnetic energy levels and ν_Q is given by the relation

$$\nu_Q=(e^2qQ/2\pi\hbar)\,[3/2I(2I-1)]\ . \tag{18}$$

q is the principal component of the electric field gradient and Q is the cesium quadrupolar moment. From the spacing of the peaks identified in Fig. 5,

$$\nu_Q=16.8\pm1\ \text{kHz}. \tag{19}$$

D. Is C_8Cs Unique?

A variety of experimental observations suggest that C_8Cs, the most cesium rich of the cesium-graphite intercalation compounds, is unique electronically.[7,10,18] Two additional, though related, observations are provided by this research:

(i) The T_1 of Cs^{133} in C_8Cs is about 8 sec at 1.3 °K compared to 27 and 48 min in $C_{24}Cs$ and $C_{36}Cs$, respectively.

(ii) The cesium Knight shift in C_8Cs is 0.29%, while in $C_{24}Cs$ and $C_{36}Cs$ it is immeasurably small or zero.

These results imply that there remains some electronic density at the cesium nuclear sites in C_8Cs, but only a negligible amount in $C_{24}Cs$ and $C_{36}Cs$ (and probably all cesium-poor stages). An estimate of the degree of ionization, determined by comparison of the Knight shift in C_8Cs to the shift in metallic cesium, gives about 55% ionization. (The ratio of the Knight shifts is about $\frac{1}{5}$. $\Delta H/H$ is proportional to the square of the wave-function density at the nucleus. The value for the degree of ionization comes from the assumption that the wave-function density at the Cs^{133} nucleus is a direct measure of the electronic density at the cesium sites.)

ACKNOWLEDGMENTS

I would like to express great appreciation for the patient guidance and constant encouragement of Professor D. F. Holcomb under whose direction this research was performed. His contributions extend beyond both this research and what little acknowledgment I can give here. I am grateful to Professor R. M. Cotts for helpful discussions in all aspects of this work. In addition, I thank J. A. Kaeck for many helpful experimental suggestions and Professor J. A. Krumhansl for assistance in applying some of the theories about graphite to my data. I also thankfully acknowledge the day to day assistance of R. L. Melcher and P. A. Lightsey. P. A. Lightsey built the boxcar integrator used in this research.

APPENDIX: DENSITY OF STATES ON A TIGHT-BINDING EXTENSION TO SLONCZEWSKI-WEISS BAND MODEL.

The energy spectrum of graphite is given by the Slonczewski-Weiss model. The four bands are given by

$$\begin{aligned} E&=\tfrac{1}{2}(E_1+E_3)\pm[\tfrac{1}{4}(E_1-E_3)^2+\gamma_0^2\sigma^2]^{1/2}\ ,\\ E&=\tfrac{1}{2}(E_2+E_3)\pm[\tfrac{1}{4}(E_2-E_3)^2+\gamma_0^2\sigma^2]^{1/2}\ , \end{aligned} \tag{A1}$$

where

$$E_1=\Delta+2\gamma_1\cos\tfrac{1}{2}\xi\ ,\qquad E_2=\Delta-2\gamma_1\cos\tfrac{1}{2}\xi\ ,$$

$$E_3=2\gamma_2\cos^2\tfrac{1}{2}\xi\ ,\qquad \sigma=\tfrac{1}{2}(\sqrt{3})\,a_0\,|\mathcal{K}|\ ,$$

$$\mathcal{K}^2=k_x^2+k_y^2\ ,\qquad \xi=c_0k_z\ .$$

a_0 and c_0 are the graphite lattice constants. The other parameters are defined in Ref. 13.

The first equation in (A1) will generate all four bands if ξ is allowed to run from 2π to -2π.

The parameters γ_3 and γ_4 of the full model have been neglected. γ_3 is the trigonal warping of the Fermi surface. Its exclusion preserves rotational symmetry, simplifying the evaluation of $\mathfrak{D}(E)$. γ_4 is the potential-energy difference between A and B

lattice sites.

The density of states $\mathfrak{D}(E)$ is given by

$$\mathfrak{D}(E)dE = [2V/(2\pi)^3] \int_E^{E+dE} d^3k \quad , \tag{A2}$$

where $\mathfrak{D}(E)$ will be in (atom eV)$^{-1}$ if V is the atomic volume $\frac{1}{8}(\sqrt{3}\ a_0^2\ c_0)$. Therefore,

$$\mathfrak{D}(E)\ dE = [\sqrt{3}\ a_0^2\ c_0/2(2\pi)^3] \int_E^{E+dE} d^3k \quad . \tag{A3}$$

A factor of 2 has been included because there are two such volumes in each zone. Exploiting the cylindrical symmetry,

$$\int d^3k = 2\pi \int d\mathcal{K}\, dk_z = (4\pi/3\ a_0^2\ c_0) \int d(\sigma^2) d\xi \tag{A4}$$

and

$$\mathfrak{D}(E) = \frac{1}{4\pi^2\sqrt{3}} \int \frac{d(\sigma^2)}{dE} d\xi \quad , \tag{A5}$$

$d(\sigma^2)/dE$ is obtained from Eq. (A1) and

$$\mathfrak{D}(E) = (1/4\pi^2\sqrt{3}\ \gamma_0^2) \int [2E - (E_1 + E_3)]\, d\xi \quad . \tag{A6}$$

The integral is performed in terms of ξ,

$$\mathfrak{D}(E) = (1/4\pi^2\sqrt{3}\ \gamma_0^2) \left[(2E - \Delta)\xi + 4\gamma_1 \sin \tfrac{1}{2}\xi - \gamma_2\xi - \gamma_2 \sin\xi \right]_{\xi_1}^{\xi_2} \quad . \tag{A7}$$

For a given E, ξ_1 and ξ_2 are the extreme values of ξ and may be determined from Eq. (A1). It will be sufficient, and quite a bit simpler, to assume that all Fermi energies will be above the region of band intermixing. In this regime, $E > (2\gamma_1 + \Delta)$ and the limits of ξ are merely 2π and -2π. Then

$$\mathfrak{D}(E) = (2/\sqrt{3}\ \pi\gamma_0^2)\ [E - \tfrac{1}{2}(\Delta + \gamma_2)] \quad . \tag{A8}$$

McClure[30] points out that $\frac{1}{2}(\Delta + \gamma_2)$ is the average energy of the four bands at the vertical zone edge. Equation (A8) resembles the result from the Wallace[12] two-dimensional density of states for the same γ_0 and average band energy.

Integrating $\mathfrak{D}(E)$,

$$N = \int \mathfrak{D}(E)\, dE = (0.368/\gamma_0^2)\ [\tfrac{1}{2}E^2 - \tfrac{1}{2}(\Delta + \gamma_2)E] \quad , \tag{A9}$$

or

$$E = \tfrac{1}{2}(\Delta + \gamma_2) \pm \tfrac{1}{2}[\ (\Delta + \gamma_2)^2 + (8\gamma_0^2 N/0.368)\ ]^{1/2} \quad . \tag{A10}$$

N is the number of donor electrons per carbon atom. The positive root is taken since adding electrons increases E. Finally,

$$\mathfrak{D}(E) = (0.368/\gamma_0^2)[\tfrac{1}{4}(\Delta + \gamma_2)^2 + (2\gamma_0^2 N/0.368)\ ]^{1/2} \quad . \tag{A11}$$

Inserting the most recent Slonczewski-Weiss parameter measurements,[31] the result becomes

$$\mathfrak{D}(E) = 0.274\ N^{1/2} \quad . \tag{A12}$$

The inclusion of γ_4 would leave the dependence on E, and hence N, unchanged.

---

*Work supported in part by the U. S. Army Research Office, Durham, N. C., through Contract Nos. DA-31-124-ARO-D-407 and DA-ARO-D-31-124-G-1071, Technical Report No. 1; and by the Advanced Research Projects Agency through the Materials Science Center at Cornell, Ithaca, N. Y., MSC Report No. 1346.

†Present address: Solid State Division, U. S. Naval Ordnance Laboratory, White Oak, Silver Spring, Md. 20910.

[1]W. Rudorff, Advan. Inorg. Chem. Radiochem. 1, 223 (1959).

[2]A. R. Ubbelohde and F. A. Lewis, *Graphite and its Crystal Compounds* (Oxford U. P., London, 1960).

[3]G. R. Hennig, Progr. Inorg. Chem. 1, 125 (1959).

[4]W. Rudorff and E. Schulze, Z. Anorg. Allgem. Chem. 277, 156 (1954).

[5]L. C. F. Blackman, J. F. Mathews, and A. R. Ubbelohde, Proc. Roy. Soc. (London) 258A, 339 (1960).

[6]S. Aronson, F. J. Salzano, and D. Bellafiore, J. Chem. Phys. 49, 434 (1968).

[7]N. B. Hannay, T. H. Geballe, B. T. Matthias, K. Andres, P. Schmidt, and D. MacNair, Phys. Rev. Letters 14, 225 (1965).

[8]D. E. Nixon and G. S. Parry, J. Phys. C 2, 1732 (1969).

[9]F. J. Salzano and S. Aronson, J. Chem. Phys. 44, 4320 (1966).

[10]F. J. Salzano and S. Aronson, J. Chem. Phys. 45, 2221 (1966).

[11]V. Jensen, D. E. O'Reilly, and T. Tsang, J. Chem. Phys. 47, 1195 (1967).

[12]P. R. Wallace, Phys. Rev. 71, 622 (1947); C. A. Coulson and R. Taylor, Proc. Phys. Soc. (London) A65, 815 (1952); W. M. Lomer, *ibid.* A227, 330 (1955).

[13]J. C. Slonczewski and P. R. Weiss, Phys. Rev. 109, 272 (1958).

[14]J. W. McClure, in *Proceedings of the Fourth Conference on Carbon* (Pergamon, New York, 1960), p. 177; J. W. McClure and L. B. Smith, in *Proceedings of the Fifth Conference on Carbon* (Pergamon, New York, 1963), Vol. II, p. 3.

[15]R. R. Haering and S. Mrozowski, Progr. Semicond. 5, 273 (1960).

[16]D. E. Nixon and G. S. Parry, J. Phys. D 1, 291 (1968).

[17]L. C. Olsen, Donald W. Douglas Laboratory Paper No. WD 1061, 1969 (unpublished).

[18]G. R. Hennig, J. Chem. Phys. 43, 1201 (1965).

[19]W. Gilbert Clark, Rev. Sci. Instr. 35, 316 (1964).

[20]A. Abragam, *The Principles of Nuclear Magnetism*

(Oxford U. P., London, 1961), p. 232.
[21]A. Narath, Phys. Rev. 179, 359 (1969).
[22]I. D. Weisman and L. H. Bennett, Phys. Rev. 181, 1341 (1969).
[23]G. P. Carver, Ph.D. thesis, Cornell University, 1970 (unpublished).
[24]C. P. Slichter, *Principles of Magnetic Resonance* (Harper and Row, New York, 1963), p. 121.
[25]A. Narath and D. C. Wallace, Phys. Rev. 127, 724 (1962).
[26]B. J. C. Van Der Hoeven, Jr., P. H. Keesom, J. W. McClure, and G. Wagoner, Phys. Rev. 152, 796 (1966).
[27]J. R. Morton, Chem. Rev. 64, 453 (1964).
[28]Y. Obata, J. Phys. Soc. Japan 18, 1020 (1963).
[29]J. Poitrenaud, J. Phys. Chem. Solids 28, 161 (1967).
[30]J. W. McClure, Phys. Rev. 108, 612 (1957).
[31]S. J. Williamson, S. Foner, and M. S. Dresselhaus, Phys. Rev. 140, 1429 (1965).

PHYSICAL REVIEW B VOLUME 2, NUMBER 7 1 OCTOBER 1970

Low-Temperature Behavior of the Hyperfine Splitting and the Absolute Sign of the Hyperfine Constant†

R. J. Richardson, Sook Lee, * and T. J. Menne
McDonnell Douglas Research Laboratories, St. Louis, Missouri 63166
(Received 1 April 1970)

An anomalous temperature dependence of the splitting between hyperfine lines for Mn^{2+} in SrF_2 has been observed at low temperatures. This behavior is explained in terms of high electron spin polarization at low temperatures and the second-order hyperfine contribution. It is shown that for SrF_2:Mn^{2+} the actual hyperfine coupling constant A is the same within experimental error at $T=77$, 4.2, and 1.3 K. In general this type of anomalous behavior of the hyperfine splitting can be used to determine the absolute sign of A for a paramagnetic ion with electronic spin $S \geq 1$ when the fine-structure splitting is vanishing or very small. For Mn^{2+} in SrF_2 the sign of A is determined to be negative.

I. INTRODUCTION

In conducting studies of the temperature dependence of the hyperfine coupling constant $A(T)$ of S-state ions in cubic crystals, it is important to make measurements of $A(T)$ in the temperature region below 77 K for the following reasons: (i) The "knee" of the curves predicted by present theories[1-5] generally falls in this region, and (ii) the presence of local modes[6] may influence the low-temperature behavior of $A(T)$. Consequently, we intended to measure $A(T)$ of $^{55}Mn^{2+}$ in the alkaline-earth fluorides for $T \leq 77$ K, since no data have been reported in this region. In the course of these investigations, we discovered an anomalous increase in the apparent magnitude of A as the temperature was lowered. We report in this paper the results of our observations and an explanation of this anomalous behavior. At the same time, we demonstrate that these measurements can be used to determine unambiguously the absolute sign of the hyperfine coupling constant of paramagnetic ions with effective spin $S \geq 1$ when the fine-structure splitting is zero or very small.

II. EXPERIMENTAL

A series of ESR investigations were performed on a single crystal of SrF_2 containing nominally 0.5 wt% of Mn^{2+} ions at 77, 4.2, and 1.3 K at 9.3 and 31.8 GHz. The two spectrometer systems employed were a modified X-band Varian spectrometer and a modified K_a-band Strand Labs spectrometer, both of which were used in conjunction with a model HR-8 Princeton Applied Research lock-in amplifier and 1000-KHz field modulation.

The ESR spectra obtained from the crystal displayed six rather broad (~35 G between the two inflections of the first derivative curve) ^{55}Mn ($I=\frac{5}{2}$) hyperfine component lines, which exhibited no resolved superhyperfine structure with the fluorine nuclei. The linewidth of each hyperfine component line and the splitting between hyperfine lines were experimentally independent of the crystal orientation with respect to the magnetic field direction.

To investigate the temperature dependence of the hyperfine coupling constant A of Mn^{2+} in the crystal at low temperatures, we measured the separation (ΔH) between points of zero first derivative of the two outermost ($m=+\frac{5}{2}$ and $m=-\frac{5}{2}$) hyperfine component lines at 77, 4.2, and 1.3 K. Table I shows the measured values of ΔH at the two indicated microwave frequencies for low microwave power levels so that the ESR lines were not saturated. It is seen that ΔH substantially increases as the temperature decreases and that it depends on the microwave frequency.

Measurements of ΔH were made as a function of

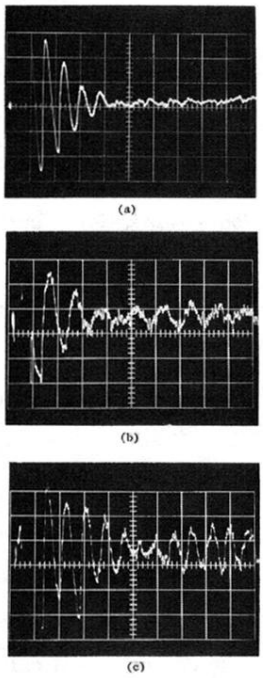

FIG. 6. Cs^{133} FID, slightly off resonance, at full magnetization in (a) C_8Cs, (b) $C_{24}Cs$, and (c) $C_{36}Cs$ at 1.3 °K. The time scale is 50 μsec per large division.